

Diamond saw dicing of Thulium channel waveguide lasers in monoclinic crystalline films

ESROM KIFLE,¹ PAVEL LOIKO,² UWE GRIEBNER,³ VALENTIN PETROV,³
PATRICE CAMY,² ALAIN BRAUD,² MAGDALENA AGUILÓ,¹ FRANCESC DÍAZ,¹
AND XAVIER MATEOS^{1,*}

¹Universitat Rovira i Virgili, Departament Química Física i Inorgànica, Física i Cristal·lografia de Materials i Nanomaterials (FICMA-FICNA)-EMaS, Campus Sescelades, E-43007 Tarragona, Spain

²Centre de recherche sur les Ions, les Matériaux et la Photonique (CIMAP), UMR 6252 CEA-CNRS-ENSICAEN, Université de Caen, 6 Boulevard du Maréchal Juin, 14050 Caen Cedex 4, France

³Max Born Institute for Nonlinear Optics and Short Pulse Spectroscopy, Max-Born-Str. 2a, D-12489 Berlin, Germany

*Corresponding author: xavier.mateos@urv.cat

Received XX Month XXXX; revised XX Month, XXXX; accepted XX Month XXXX; posted XX Month XXXX (Doc. ID XXXXX); published XX Month XXXX

A surface channel waveguide laser is produced by diamond saw dicing of a 15 μm -thick 10 at.% $\text{Tm:KY}_{1-x-y}\text{Gd}_x\text{Lu}_y(\text{WO}_4)_2$ monoclinic double tungstate thin film grown by Liquid Phase Epitaxy on an undoped $\text{KY}(\text{WO}_4)_2$ substrate. The waveguide propagation losses are 1.1 ± 0.5 dB/cm. When pumped at 802 nm, laser operation is achieved with a maximum output power of 262 mW at 1833 nm with a record slope efficiency of 82.6% (versus the absorbed pump power) in a TE_{10} spatial mode (linear laser polarization, $E \parallel N_m$). Diamond-saw-dicing of double tungstate epitaxies is a promising technology for manufacturing waveguides for sensing applications.

<http://dx.doi.org/10.1364/OL.99.099999>

Surface passive and active waveguides (WGs) are promising for functionalization of their surface which is relevant for applications in sensing technology. Such devices rely on the evanescent-field coupling of the laser mode with the deposited material. Such a design compared with devices operating in transmission-mode, greatly enhances the interaction length and reduces the passive losses. Moreover, it features a small depth of light penetration into the deposited material. Surface WGs can be functionalized with a nonlinear material (saturable absorber) for generation of ns pulses via a passive Q-switching mechanism [1-3]. They can be used for bio- and environmental sensing and spectroscopy as well [4]. For this purpose, the near-mid-infrared spectral range of 2-3 μm is particularly interesting as it contains absorption lines of molecules such as H_2O , CO , CO_2 , NO_2 , etc.

Laser emission around 2 μm is typically achieved using Thulium (Tm^{3+}) or Holmium (Ho^{3+}) ions. In the former case, it originates from

the ${}^3\text{F}_4 \rightarrow {}^3\text{H}_6$ transition. Tm^{3+} ions feature an absorption band at ~ 0.8 μm (to the ${}^3\text{H}_4$ state) and their pump quantum efficiency may reach 2 due to an efficient cross-relaxation process (CR), ${}^3\text{H}_4 + {}^3\text{H}_6 \rightarrow {}^3\text{F}_4 + {}^3\text{F}_4$. For Tm WG lasers, the monoclinic double tungstate (MDT) crystals, $\text{KRE}(\text{WO}_4)_2$, where RE = Gd, Y or Lu, are well-recognized materials [5]. They have attractive spectral properties in polarized light [5,6] and can support high Tm^{3+} concentrations leading to efficient CR accompanied with weak quenching of the 2 μm luminescence [7]. Waveguiding thin films of MDT are typically produced by Liquid Phase Epitaxy (LPE) on undoped (bulk) substrates [8]. Micro-structuring of such active layers was performed by Ar^+ -ion etching and a compositionally “mixed” Tm:MDT buried channel WG laser has been scaled to 1.6 W at 1.84 μm with a slope efficiency of $\sim 80\%$ [9]. Low propagation losses of 0.2 dB/cm have been measured in such WGs [10].

Ar^+ -ion etching is nevertheless a complicated technology which requires a heavy equipment. Recently, precision diamond saw dicing, a well-known and commercialized technology for silicon wafer cutting has been proposed for the fabrication of surface WGs. It has also been used for the fabrication of WGs based on polymers [11] and crystalline thin films [12,13]. In Ref. [12], a Nd^{3+} :Sapphire ridge WG laser generated 322 mW at 1092 nm with a slope efficiency of only $\sim 12\%$ due to relatively high scattering losses of 6 dB/cm. Using a Nd:YAG ridge WG, Y. Jia *et al.* extracted 84 mW at 1064 nm with a slope efficiency of 43% and a WG propagation loss of 1.7 dB/cm [13]. WGs in LiNbO_3 and KTiOPO_4 were also fabricated by diamond saw dicing [14-16] featuring WG propagation losses of about 1 dB/cm. They were used for second-harmonic generation leading to green emission. Very recently, diamond saw dicing was used for the production of channel WGs in tetragonal $\text{Tm,Gd:LiYF}_4 / \text{LiYF}_4$ epitaxial films [17].

In the present paper, we aim to demonstrate the first Tm^{3+} channel WG laser based on low-symmetry (monoclinic) crystal and diamond saw dicing featuring moderate propagation losses and high slope efficiency almost approaching the theoretical limit, as a platform for surface functionalized devices. The application of diamond saw dicing

for MDT thin films is not a trivial task because of the strong anisotropy of thermo-mechanical properties of these materials.

The Tm^{3+} -doped active layer (thin film) with a composition of $\text{KY}_{0.61}\text{Gd}_{0.22}\text{Lu}_{0.07}\text{Tm}_{0.10}(\text{WO}_4)_2$ (actual Tm^{3+} concentration $N_{\text{Tm}} = 5.83 \times 10^{20}$ at/cm³) was grown on an undoped bulk $\text{KY}(\text{WO}_4)_2$ substrate by Liquid Phase Epitaxy (LPE). The Gd^{3+} and Lu^{3+} ions were added to reduce the lattice mismatch and to promote a positive refractive index contrast between the layer and the substrate [18]. The substrate was double-side-polished and oriented with its faces being orthogonal to the (010) axis. The bulk $\text{KY}(\text{WO}_4)_2$ crystal was grown by the Top-Seeded Solution Growth (TSSG) method [5]. For the LPE growth, potassium ditungstate, $\text{K}_2\text{W}_2\text{O}_7$, was used as a solvent. The solute / solvent ratio was 7 / 93 mol% and the corresponding saturation temperature T_S was 1160.9 K. The LPE growth was performed at 3 K below T_S for 2.5 hours resulting in a uniform layer. More details can be found elsewhere [5]. The layer was further polished to a thickness of 15.3 μm , as confirmed by Environmental Scanning Microscopy (ESEM), Fig. 1(a). The epitaxy (abbreviated as $\text{Tm:KYW} / \text{KYW}$) was oriented for light propagation along the N_g optical indicatrix axis (KYW is an optically biaxial crystal). Both edges of the epitaxial layer were polished to laser quality and remained uncoated.

The measured lifetime of the $^3\text{F}_4$ Tm^{3+} multiplet was 0.79 ms which is only slightly shorter than the radiative one, 1.11 ms [6]. For Tm:KYW , the peak stimulated-emission (SE) cross-section $\sigma_{\text{SE}}(^3\text{F}_4 \rightarrow ^3\text{H}_6)$ is 4.2×10^{-20} cm² at 1.84 μm [6].

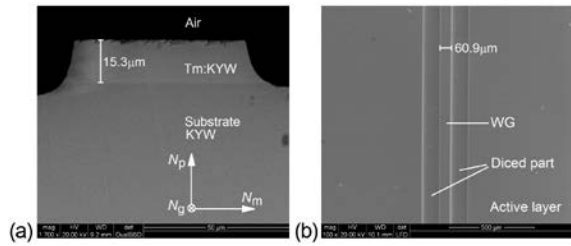


Fig. 1. ESEM images of the (a) polished end-facet and (b) top surface of the diced 10 at.% $\text{Tm:KYW} / \text{KYW}$ epitaxy.

The surface channel WG was produced using a precision dicing saw (Disco DAD 321). A metal bonded blade (6000 grit, outer diameter: 54 mm, thickness: 0.1 mm) with synthetic diamonds was used. The dicing parameters were optimized by performing multiple cuts on similar test samples. The feed rate (the distance travelled by the blade in its each revolution) was determined from the blade rotation and translation speeds. Values in the range of 0.15 – 0.3 $\mu\text{m}/\text{rev}$ (limited by the maximum rotation speed) were tested by assessing the surface roughness of the cuts. The smaller feed rates provided the lowest surface roughness. Thus, we selected the feed rate of 0.15 $\mu\text{m}/\text{rev}$ (rotation speed: 40,000 revolutions per minute (rpm), horizontal translation speed: 0.1 mm/s). No vertical blade movement was applied. The dicing depth was optimized to be ~ 20 μm by inspection of the channel side walls using a confocal microscope. For smaller depths, there was a significant chipping at the sample end-facets. During the dicing, the blade and the sample were cooled with a room-temperature deionized water flowing at a rate of 1 liter/min. It served as a lubricant during the cutting process and helped to remove the cutting debris from the region currently being diced.

The produced surface channel (ridge) WG was analyzed with ESEM, Fig. 1. The width of the WG was 60.9 ± 0.5 μm (it was selected according to the dicing tests leading to low roughness of the cut). The side walls of the WG were slightly rounded and their root-mean-square (rms)

roughness was < 0.15 μm . No cracks were observed in the active layer and in the substrate. The dicing depth was about 20 μm , thus completely removing the active layer. The length of the WG l was 3.5 mm.

The scheme of the laser set-up is shown in Fig. 2. The sample was mounted on a glass support and it was passively cooled. Bulk laser mirrors were used to build the laser cavity consisting of a flat pump mirror (PM) coated for high transmission at 0.7–1 μm and for high-reflection at 1.8–2.1 μm , and a flat output coupler (OC) with a transmission T_{OC} at 1.8–2.1 μm ranging from 1.6% to 30%. Laser operation without OC (simple Fresnel reflection from the WG output facet corresponding to $T_{\text{OC}} = 89\%$) was also tested. Both PM and OC were placed close to the WG end-facets. No index-matching liquid was used.

The WG was pumped by a CW Ti:Sapphire laser tuned to 802 nm ($^3\text{H}_6 \rightarrow ^3\text{H}_4$ Tm^{3+} transition). The pump polarization in the active layer corresponded to $E \parallel N_m$. The incident pump power was varied by a gradient neutral density filter. The pump was focused by a microscope objective (10 \times , N.A. = 0.28) through the PM. The measured pump spot size in the focus $2w_p = 40 \pm 5$ μm . The pump coupling efficiency η_{coupl} was $42 \pm 1\%$ (as determined from pump-transmission measurements at 0.84 μm , out of Tm^{3+} absorption). The pump absorption $\eta_{\text{abs,L}}$ measured at the laser threshold pump power was above 99% in agreement with our rate-equation modeling taking into account the possible ground-state bleaching. For the actual Tm^{3+} concentration and the absorption cross-section σ_{abs} of 5.2×10^{-20} cm² at 802 nm, the small-signal absorption $\eta_{\text{abs},0} = 1 - \exp(-\sigma_{\text{abs}} N_{\text{Tm}} l)$ is almost unity. The observed guided mode at the pump wavelength was TE_{10} .

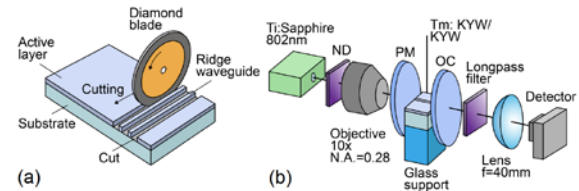


Fig. 2. (a) Scheme of the diamond saw dicing of ridge WGs; (b) diced surface channel 10 at.% $\text{Tm:KYW} / \text{KYW}$ WG laser: ND – gradient neutral density filter, PM – pump mirror, OC – output coupler.

The output laser emission was filtered from the non-coupled pump radiation using a long-pass filter (Thorlabs, FEL1000). The spatial profile of the laser mode was measured using a 40 mm spherical lens and a FIND-R-SCOPE near-IR camera. A calibration target was used to determine the actual beam size at the WG output facet. The laser spectra were measured using an optical spectrum analyzer (Yokogawa, model AQ6375B).

Laser operation for the channel surface $\text{Tm:KYW} / \text{KYW}$ WG has been achieved for all studied OCs and also without any OC, Fig. 3(a). In the latter case, a maximum CW output power of 262 mW at 1833 nm with a record slope efficiency η of 82.6% (vs. the absorbed pump power P_{abs}) was achieved. Such a high value of η is due to the efficient cross-relaxation among Tm^{3+} ions in the active layer as expected for such a high doping concentration (10 at%), leading to a pump quantum efficiency η_q of > 1.96 [7,9]. Thus, the measured slope efficiency is close to the theoretical limit [9], $\eta < \eta_{\text{mode}} \cdot \eta_{\text{OC}} \cdot \eta_q \cdot \eta_{\text{StL}} = 79 \pm 2\%$, where η_{mode} is the mode overlap efficiency, $\eta_{\text{OC}} = \ln[1 - T_{\text{OC}}] / \ln[(1 - T_{\text{OC}}) \cdot (1 - 2L)] = 92 \pm 2\%$ is the output-coupling efficiency ($2L$ is the roundtrip passive loss, see below), $\eta_{\text{StL}} = \lambda_p / \lambda_L = 43.8\%$ is the Stokes efficiency under lasing conditions. One of the factors limiting the laser efficiency in highly-doped quasi-three-level materials is the residual reabsorption at the wings of the pump mode [9]. However,

this effect is expected to be weak for high pump intensities well above the laser threshold. The laser threshold was at $P_{\text{abs}} = 214$ mW and the optical-to-optical efficiency η_{opt} was 21.0% (vs. the incident pump power). For smaller T_{OC} , η gradually decreased. The lowest laser threshold (147 mW) corresponded to 1.5% T_{OC} .

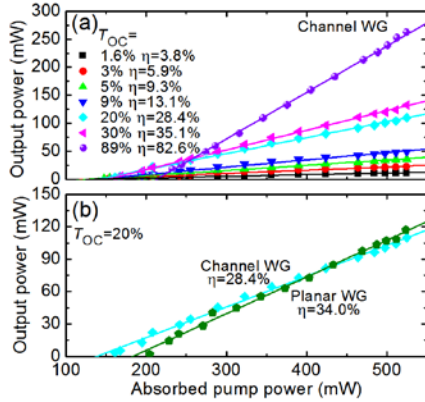


Fig. 3. (a,b) Input-output dependences of the planar and diced surface channel 10 at.% Tm:KYW / KYW WG lasers: (a) channel WG, various T_{OC} , symbols – experimental data, lines – their fits for the calculation of the slope efficiency (η), TE₁₀ spatial mode; (b) comparison of laser performance for planar and channel WGs for $T_{\text{OC}} = 20\%$. The laser polarization is $\mathbf{E} \parallel N_m$.

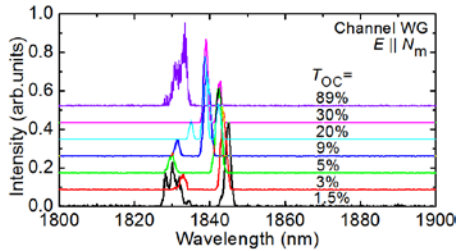


Fig. 4. Typical laser emission spectra of the diced surface channel 10 at.% Tm:KYW / KYW WG laser (measured at $P_{\text{abs}} \sim 0.5$ W). The laser polarization is $\mathbf{E} \parallel N_m$.

For comparison, the planar WG operation (in the non-diced part) was studied. In Fig. 3(b), we compared the laser performance achieved for channel and planar WGs (for $T_{\text{OC}} = 20\%$). Planar WG laser exhibited higher threshold (204 mW vs. 160 mW for the channel WG) due to the larger laser mode size in the non-guided direction and slightly higher slope efficiency (34.0% vs. 28.4% for the channel WG) due to the lower WG propagation losses in the absence of dicing. In general, ridge WGs are more attractive as (i) they provide a lower laser threshold, (ii) they may provide single-transverse-mode operation and (iii) they can be pumped by single-mode-fiber light sources (e.g., fiber lasers or fiber-coupled diodes).

For all OCs, the input-output dependences in Fig.3 are linear indicating no detrimental thermal effects. No thermal fracture of the sample was observed. The power scaling was limited by the available pump power.

The laser emission was linearly polarized ($\mathbf{E} \parallel N_m$) due to the gain anisotropy [5,6]. For all OCs, the emission occurred at around the wavelength of 1.84 μm , Fig. 4, which corresponds to a local peak in the gain spectra of Tm³⁺ ions in KYW for high inversion rates $\beta > 0.4$. A

slight blue-shift of the spectra with increasing T_{OC} is due to the quasi-three-level nature of the Tm³⁺ laser scheme (it is related to decreased reabsorption with increasing β [5]).

The WG propagation losses were determined using a Caird plot modified for the case of high output coupling [19,20], namely, by plotting $1/\eta$, vs. the inverse of the output-coupling loss, $1/\gamma_{\text{OC}}$, where $\gamma_{\text{OC}} = -\ln(1-T_{\text{OC}})$, Fig.5(a). The corresponding dependence can be expressed as $1/\eta = 1/\eta_0(1+2\gamma/\gamma_{\text{OC}})$, where η_0 is the intrinsic slope efficiency and $\gamma = -\ln(1-L)$. The Caird analysis is correct when the laser emission wavelength is nearly constant for all studied OCs [20]. This condition is satisfied in our case, see Fig. 4. The WG propagation loss was calculated as $\delta = 4.34L/l = 1.1 \pm 0.5$ dB/cm. This value is slightly higher than that determined recently for a 5 at.% Tm:KYW/KYW planar WG [21], 0.7 ± 0.2 dB/cm, which is assigned partially to higher Tm³⁺ doping and mostly to the roughness of the WG walls induced by the dicing.

The analysis of mode guidance conditions for the surface channel WG was performed at 1.84 μm using the software from Ref. [22], Fig. 5(b). The refractive indices of the active layer $n_{m(\text{layer})}$ and the substrate $n_{m(\text{substrate})}$ are 2.0056 and 2.0040, respectively, so that the refractive index contrast Δn is 1.6×10^{-3} , as calculated using the Sellmeier formulas [23]. For the studied WG, four TE modes can be supported, from TE₀₀ to TE₃₀. Single transverse mode operation is expected for WG width d of 15 - 28 μm .

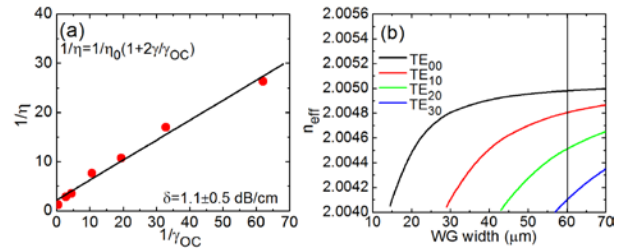


Fig. 5. Surface channel 10 at.% Tm:KYW/KYW WG: (a) modified Caird plot (inverse of the slope efficiency, $1/\eta$, vs. inverse of the output-coupling loss, $1/\gamma_{\text{OC}}$); (b) analysis of mode guidance conditions (WG thickness t : 15.3 μm , WG width d : 10-70 μm , $\lambda = 1.84 \mu\text{m}$, $\mathbf{E} \parallel N_m$). Vertical line indicates the studied WG ($d = 60.9 \mu\text{m}$).

The results on the laser mode profiles are shown in Fig. 6. For the channel WG laser, by slightly changing the distance between the PM and the WG input facet, it was possible to observe laser action in two modes (TE₁₀ and TE₃₀), with the highest output power in the former case, as plotted in Fig. 3(a). The measured mode profiles are shown in Fig. 6(a,c) and they agree well with the calculated mode result, Fig. 6(b,d). For the planar WG, the laser beam had a stripe-like profile extended in the horizontal direction, Fig. 6(e). Its 1D intensity profile in the vertical direction was well fitted with a Gaussian function (according to the mode guidance condition calculation, one mode is supported). In the horizontal direction, an additional mode confinement is most probably provided by a combination of gain-guiding and thermal lensing which is positive for N_g -cut Tm:KYW [24]. To model this mode profile numerically, Fig. 6(f), we assumed a channel WG with a width equal to the mean pump diameter in the horizontal plane.

The previously reported channel WG lasers based on MDTs were produced by a combination of LPE and Ar⁺-ion etching for microstructuring of the films or femtosecond direct laser writing (fs-DLW). A Tm:KY_{1-x}Y_xGd_xLu_y(WO₄)₂ / KY(WO₄)₂ buried channel WG laser generated 1.6 W at 1.84 μm with $\eta = 81 \pm 3\%$ [9]. In the present paper, we report on a similar laser slope efficiency using a surface channel WG. The output power in our case was limited by the available

pump source. Moreover, diamond saw dicing is an easier and less technologically demanding process than Ar^+ -ion etching. Regarding fs-DLW, lower output power (136 mW at 1844 nm) and slope efficiency (34.2%) were reported [25].

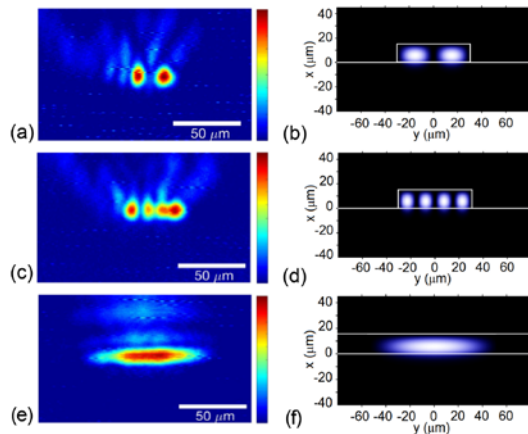


Fig. 6. (a-f) Measured (left images) and calculated (right images) mode profiles of the 10 at.% Tm:KYW / KYW surface channel and planar WG lasers: (a,b) channel WG, TE_{10} mode; (c,d) channel WG, TE_{30} mode; (e,f) planar WG. The laser polarization ($\mathbf{E} \parallel N_m$) is horizontal. The measurements are performed for $T_{\text{OC}} = 20\%$ at $P_{\text{abs}} \sim 0.5$ W.

To conclude, we report on the successful fabrication of an active (Tm^{3+} -ion-doped) surface channel (ridge) WG by combining the LPE technology for monoclinic crystals and precision diamond saw dicing. A highly-doped WG provided moderate propagation losses of 1.1 ± 0.5 dB/cm due to the low roughness of the WG walls and very high slope efficiency in excess of 80% due to efficient Tm^{3+} - Tm^{3+} cross-relaxation. The laser operated in a TE_{10} mode while single-mode (TE_{00}) operation is possible for WGs with reduced widths. The designed WGs are promising for functionalization of their top surface by deposition of optically nonlinear materials, e.g., graphene or single-walled carbon nanotubes, serving as saturable absorbers based on evanescent field coupling leading to passively Q-switched (pulsed) operation. Another possible application of such active WGs can be bio- and environmental sensing.

Funding. Spanish Government (MAT2016-75716-C2-1-R (AEI/FEDER/UE), TEC 2014-55948-R); Generalitat de Catalunya (2014SGR1358).

Acknowledgment. F. D. acknowledges additional support through the ICREA academia award 2010ICREA-02 for excellence in research. E. K. acknowledges financial support from Generalitat de Catalunya (grants 2016FI_B00844, 2017FI_B100158).

References

- J. W. Kim, S. Y. Choi, D. I. Yeom, S. Aravazhi, M. Pollnau, U. Griebner, V. Petrov, and F. Rotermund, *Opt. Lett.* **38**, 5090 (2013).
- Y. Tan, R. He, J. Macdonald, A. K. Kar, and F. Chen, *Appl. Phys. Lett.* **105**, 101111 (2014).
- A. Choudhary, S. J. Beecher, S. Dhingra, B. D'Urso, T. L. Parsonage, J. A. Grant-Jacob, P. Hua, J. I. Mackenzie, R. W. Eason, and D. P. Shepherd, *Opt. Lett.* **40**, 1912 (2015).
- C. Grivas, *Progr. Quantum Electron.* **45**, 3 (2016).
- V. Petrov, M. C. Pujol, X. Mateos, Ò. Silvestre, S. Rivier, M. Aguiló, R. M. Solé, J. H. Liu, U. Griebner, and F. Díaz, *Laser Photonics Rev.* **1**, 179 (2007).
- A. E. Troshin, V. E. Kisel, A. S. Yasukevich, N. V. Kuleshov, A. A. Pavlyuk, E. B. Dunina, and A. A. Kornienko, *App. Phys. B* **86**, 287 (2007).
- X. Mateos, P. Loiko, J.M. Serres, K. Yumashev, U. Griebner, V. Petrov, M. Aguiló, and F. Díaz, *IEEE J. Quantum Electron.* **53**, 1700110 (2017).
- W. Bolaños, J. J. Carvajal, X. Mateos, E. Cantelar, G. Lifante, U. Griebner, V. Petrov, V. L. Panyutin, G. S. Murugan, J. S. Wilkinson, M. Aguiló, and F. Díaz, *Opt. Express* **19**, 1449 (2011).
- K. van Dalfsen, S. Aravazhi, C. Grivas, S. M. García-Blanco, and M. Pollnau, *Opt. Lett.* **39**, 4380 (2014).
- K. van Dalfsen, S. Aravazhi, D. Geskus, K. Wörhoff, and M. Pollnau, *Opt. Express* **19**, 5277 (2011).
- G. F. Chen, X. Zhao, Y. Sun, C. He, M. C. Tan, and D. T. Tan, *Sci. Rep.* **7**, 3366 (2017).
- S. H. Waeselmann, C. E. Rüter, D. Kip, C. Kränkel, and G. Huber, *Opt. Mater. Express* **7**, 2361 (2017).
- Y. Jia, C. E. Rüter, S. Akhmalaliev, S. Zhou, F. Chen, and D. Kip, *Opt. Mater. Express* **3**, 433 (2013).
- N. Courjal, B. Guichardaz, G. Ulliac, J.-Y. Rauch, B. Sadani, H.-H. Lu, and M.-P. Bernal, *J. Phys. D Appl. Phys.* **44**, 305101 (2011).
- C. Chen, C. E. Rüter, M. F. Volk, C. Chen, Z. Shang, Q. Lu, S. Akhmalaliev, S. Zhou, F. Chen, and D. Kip, *Opt. Express* **24**, 16434 (2016).
- J. Sun and C. Xu, *Opt. Lett.* **37**, 2028 (2012).
- P. Loiko, R. Soulard, G. Brasse, J.-L. Doulan, B. Guichardaz, A. Braud, A. Tyazhev, A. Hideur, and P. Camy, *Opt. Express* **26**, 24653 (2018).
- S. Aravazhi, D. Geskus, K. van Dalfsen, S. A. Vázquez-Córdova, C. Grivas, U. Griebner, S. M. García-Blanco, and M. Pollnau, *Appl. Phys. B* **111**, 433 (2013).
- J. Morris, N. K. Stevenson, H. T. Bookey, A. K. Kar, C. T. A. Brown, J.-M. Hopkins, M. D. Dawson, and A. A. Lagatsky, *Opt. Express* **25**, 14910 (2017).
- J. A. Caird, S. A. Payne, P. R. Staber, A. J. Ramponi, L. L. Chase, and W. F. Krupke, *IEEE J. Quantum Electron.* **24**, 1077 (1988).
- E. Kifle, X. Mateos, P. Loiko, S.Y. Choi, J. E. Bae, F. Rotermund, M. Aguiló, F. Díaz, U. Griebner, V. Petrov, *Opt. Express* **26**, 4961 (2018).
- O. V. Ivanova, R. Stoffer, and M. Hammer, A variational mode solver for optical waveguides based on quasi-analytical vectorial slab mode expansion, University of Twente, technical report, pp. 1-19 (2009).
- P. Loiko, P. Segonds, P.L. Inácio, A. Peña, J. Debray, D. Rytz, V. Filippov, K. Yumashev, M.C. Pujol, X. Mateos, M. Aguiló, F. Díaz, M. Eichhorn, and B. Boulanger, *Opt. Mater. Express* **6**, 2984 (2016).
- M.S. Gaponenko, P.A. Loiko, N.V. Gusakova, K.V. Yumashev, N.V. Kuleshov, and A.A. Pavlyuk, *Appl. Phys. B* **108**, 603 (2012).
- E. Kifle, P. Loiko, X. Mateos, J. R. Vázquez de Aldana, A. Ródenas, U. Griebner, V. Petrov, M. Aguiló, and F. Díaz, *Opt. Mater. Express* **7**, 4258 (2017).